Chinese Chemical Letters 35 (2024) 109036

Contents lists available at ScienceDirect

Chinese Chemical Letters

journal homepage: www.elsevier.com/locate/cclet

Mobile mini-fluorimeter for antibiotic aptasensing based on surface-plasmonic effect of burlike nanogolds enhanced by digitized imaging diagnosis

Tiantian Man[a], Fulin Zhu[a], Yaqi Huang[a], Yuhao Piao[b], Yan Su[a], Shengyuan Deng[b,*], Ying Wan[a,*]

[a] School of Mechanical Engineering, Nanjing University of Science and Technology, Nanjing 210094, China
[b] Key Laboratory of Metabolic Engineering and Biosynthesis Technology, Ministry of Industry and Information Technology, School of Environmental and Biological Engineering, Nanjing University of Science and Technology, Nanjing 210094, China

ARTICLE INFO

Article history:
Received 13 March 2023
Revised 3 August 2023
Accepted 31 August 2023
Available online 3 September 2023

Keywords:
Chloramphenicol and enrofloxacin
Aptasensor
Gold nanoburs
Smartphone fluorimetric suite
Digitized image postprocessing

ABSTRACT

Antibiotic abuse now poses a grave threat to global ecology and bestirs public concerns about the residue issue in daily necessities. The traceability measurements along supply chain or logistic circulation have become increasingly essential given the labile nature of diverse synthetic residuals on site. In an attempt to answer this urgency, here a miniaturized fluorometric aptasensor prototype was contrived that catered to the point-of-care screening norm for two typical additives: chloramphenicol and enrofloxacin. The key target-indicating module worked *in vitro* based on the competitive binding-induced fluorescence recovery of fluorescein-labeled aptamers, which were photobleached beforehand in the format of double helix on burlike nanogold carriers. The "prickly" geometry of the latter not just enriched the capture probes at preferentially substrate-accessible spires; but also contributed to a tip-enhanced surface plasmon effect, sensitizing the signal-on during the duplex dissociation even at nanomolar threshold of the analytes. On the other hand, to encompass a full portable, a set of optical devices were mounted within a 3D-printed cartridge (adaptor) to converge the light beam and route it towards the detector, for which the smartphone camera came up in handy with a home-developed App for calibrating the emissive brightness. Enlightened by the high-dynamic-range compression, an imaging diagnostic algorithm was built in to grid and digitize each slide in the album for augmented detection performance. Thus, a novel bio-to-silico integration was invented that capable of *in situ* rapid reporting on the antibiotic presence with high sensitivity and selectivity. Further field practices in spiked milk on sales proved the precision and rudimentary feasibility of the well-assembled model of appliance, thus holding nice prospects in nonexpert (*e.g.*, family and local community) utilities for foodborne antibiotic identification.

Unchecked residues of abused antibiotics have not only contaminated hydrographic net and intercontinental soils, but been enriched upward food chain to threaten public health atop [1–3]. To be exemplified, chloramphenicol (CHL) and enrofloxacin (ENR), as broad-spectrum antimicrobials in veterinary [4–6], caused a complication of cumulative effects at multi-levels from genetic mutation, gastrointestinal flora imbalance to bone marrow suppression [7–10], *etc.* Setting up checkpoints to oversee the resourcing of terminal products did prove to be a high-standard policy for containing the overuse. Currently, there are authorized central laboratories responsible for those processed inspections. However, routine cumbersome instrumentation, *e.g.*, liquid chromatography-mass spectrometry [11], and capillary electrophoresis [12], could hardly be up to the newly demanded traceability evaluation; needless to say, the labor-intensive derivatization of perishable samples [13]. Given the volatile nature of diverse environmental metabolites of synthetic additives, on-site rapid reporting on the antibiotic presence would surely boost the screening flow as well as its quantitative true positive rate. More importantly, such a close-to-end user practice appears easily to evoke the vigilance of consumers.

In an attempt to fulfil the aforementioned needs, analysts had recourse to the cutting-edge norm "the point-of-care testing (POCT)" in clinical chemistry [3], and adapted its pillar tech-

* Corresponding authors.
E-mail addresses: sydeng@njust.edu.cn (S. Deng), wanying@njust.edu.cn (Y. Wan).

https://doi.org/10.1016/j.cclet.2023.109036
1001-8417/

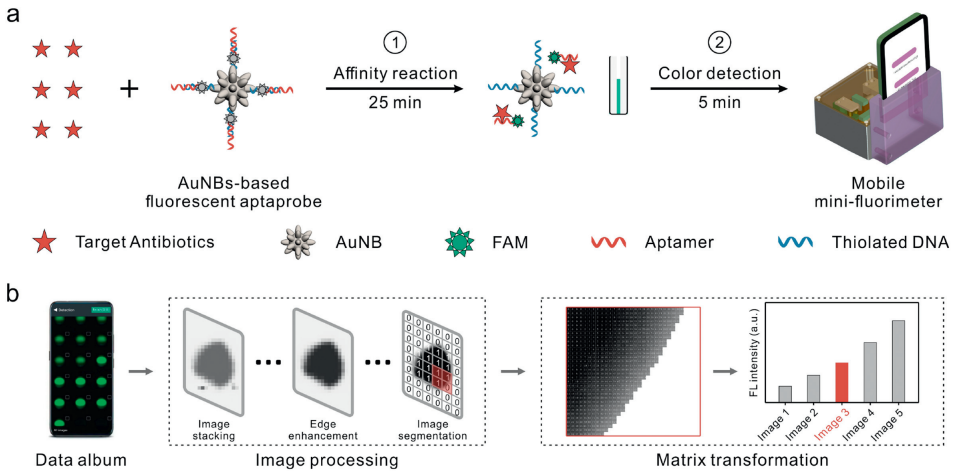

Scheme 1. Proof-of-concept walkthrough of the mobile mini-fluorometric platform for CHL and ENR determinations. (a) Design of the aptaprobe, that partially complementary double-stranded DNA (dsDNA) are anchored on the conical surface of a gold nanobur (AuNB) *via* Au−S bonding with the thiolated single-stranded capture (ssDNA, blue). The other is a FAM-terminated aptamer (red), of which the fluorophore is quenched due to its excitonic energy transfer to the proximal AuNB. The tighter affinity with antibiotics releases the aptameric primer off in company with a fluorescent switch-on within 25 min. This reaction occurs in a cuvette installed in a spectrometer chamber. Its optical configuration is illustrated in the block diagram of Fig. S3 (Supporting information). (b) Digitized imaging diagnostic protocol. One saved collection of 480-nm excited exposures at fixed frame rate is interstacked, edge-sharpened and partitioned at pixel resolution for noise suppression. Next, the most expected area out of the alignment over sampled slides is superposed into a grayscale array, which is converted mathematically (a default Gamma setting for RGB-to-grayscale transition utilized the weighted average: $0.299 \times R + 0.587 \times G + 0.114 \times B$) into a net FL illuminance. Such sequential processing takes another 5 min per run.

niques of colorimetry [14,15] and electrochemistry [16–18] for either quality spot checks on the shop or logistic monitoring at the tollgate. Pioneering works in regard to such translational researches involve the swift electrochemical evaluator on pesticides [19] and the state-of-the-art self-powered antibiotic sieving [20]. Whichever scenario, the limited local market around a satellite base makes miniaturized antibiotic sensors favorite at their highlights of platform-wide multitasking capacity as well as affordable (learning) cost. Narrowing down by both features, the specific immunofluorescence fell less qualified for the risk of denatured antibody in nonphysiological milieux [21]. Instead, the adversity-resilient aptamers step up in good competence especially for small ligand binding events [22–24], typically, the DNA-kanamycin affibody in phosphorescent label-free analysis [25]. Focusing upon this type of upstream bio-recognizers, flexible signal-indicating modules can be mapped out. Yet being prioritized on reactive robustness in the black box style, classic polymerase chain or rolling circle replication would not say a totally hands-off amplification for amateurs of little bio-major. In light of this, engineers turned to relatively more result-oriented physical sensitizers [26], that can be based on material electronics of nanotags, or analog-to-digital conversion and identification. Together, the adaptive integration of these elements would encompass a systematic solution towards the desired antibiotic diagnosis.

Herein, by virtue of multidisciplinary advancement in POCT industry, a prototyped biosensor was contrived that catered to the urgency for dual most disseminated antibiotics, CHL and ENR. Modularly as Scheme 1, (1) the key target transducer worked *in vitro* by the competitive binding-induced fluorescence (FL) recovery of dye (FAM)-labeled aptamers, that photobleached beforehand in the double-helix format on a new type carrier, burlike nanogold (AuNB). Its prickly geometry not just localized capture probes at preferentially substrate-accessible spires; but also enabled a tip-enhanced surface plasmon effect, intensifying turn-on modality during the duplex dissociation even at nanomolar threshold of analytes. (2) To encompass a fully portable, a set of optical devices was mounted inside a 3D-printed cartridge to converge the emission beam routing towards the detector, *i.e.*, a smartphone camera with an App brightness readout. (3) Inspired by high-dynamic-range compression, a visual statistics algorithm was programed to align, grid and digitize multi-framed albums for high fidelity and augmented assay performance. Combining as a trinity, a bio-to-silico gizmo was assembled that capable of *in situ* short-term CHL/ENR detection with nice sensitivity and precision in spiked milk. Albeit rudimentarily feasible, this compact analyzer holds the potency of nonexpert utilities in food security.

Stellate-like AuNBs were selected to underlie the fluorescent aptaprobe due to their unique surface plasmon resonance (SPR) property that stemmed from secondary crystalization [27], which earns themselves an edge over the common spherical gold nanoparticles at orderly distributed shell hotspots of relatively more plasmonic convergency, *i.e.*, greater hot-carrier yields [28,29]. Such a perk has already been exploited for optoelectronic devices [24,28], and nanoscale theranostics [30,31]. To be specified, the so-called DNA confinement was conformed to prepare AuNBs from polyA-spherized 13-nm seeds, whereafter costabilized by polyvinylpyrrolidone (PVP) plus the reducing agent hydroxyl-amine (Fig. S1 in Supporting information). Onto this precursor, single-stranded P2 (Table S1 in Supporting information) was ligated *via* a surfactant-free strategy under pH assistance [32,33], which hybridized partly then with the luminophor-tagged P1 to finish the basic antibiotic-responsive unit (Fig. 1a). Transmission electron microscopic (TEM) images tell the size of AuNBs to be ~50 nm with exterior tiny bulges (Fig. 1b and Fig. S2a in Supporting information). Besides, in dynamic light scattering (DLS), AuNBs that carry thiolated primers (denoted AuNBs-P2/P4) were highly dispersive (polydispersity index: 0.016, Fig. S2b in Supporting information). Their zeta potentials fall in the range of [−19.6, −24.9] mV, signifying heavy interparticle repellence among negative-charged nucleotidyl surfaces (Fig. 1c). In respect to the claimed key feature of SPR, the extremum in ultraviolet-visible (UV–vis) absorption of AuNBs(-P2) red-shift obviously from $(\lambda_{ab})_{max} = 518$ nm of pristine AuNPs to 618 nm (Fig. 1d), since the latter did grow in both geometry and roughness [28]. Furthermore, the attachment of P1 quenched its labeled FAM intensity at $(\lambda_{em})_{max} = 517$ nm by >80% upon AuNBs-P2 (Fig. 1e). Such emissive interaction between dye and AuNB lays the mechanistic foundation of aptasensing. By the way, the apparent number of immobilized P1 on the individual AuNB was formulated as Eq. S2 from Figs. S3 and S4 (Supporting information) that approximated to be 1389.

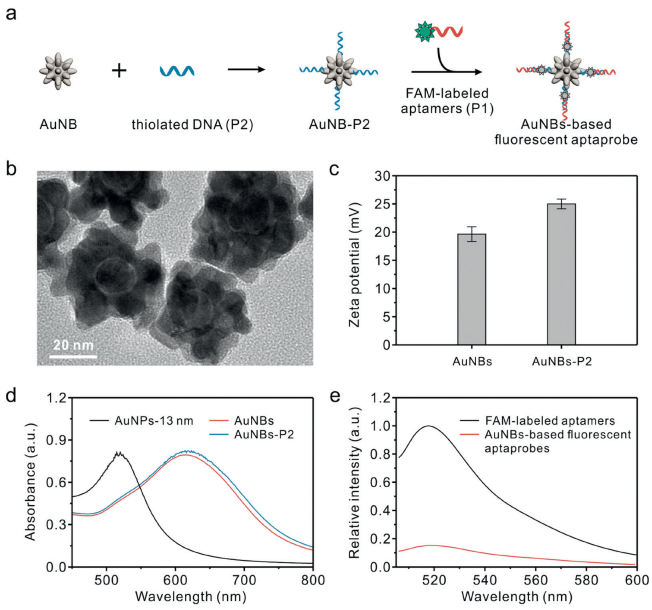

Fig. 1. (a) Workflow regarding the aptaprobe preparation with AuNB as the starting material. (b) TEM micrograph of AuNBs. (c) Zeta potential of AuNBs before and after P2-SH tethering (error bars stand for standard deviations (SD), over $n = 3$). (d) UV–vis absorption spectra of normal AuNPs, bare AuNBs and AuNBs-P2. (e) Photoluminescence profiles of FAM-P1 before and after its association with AuNBs-P2 when excited optimally at $(\lambda_{ex})_{opt} = (\lambda_{ab})_{max}$.

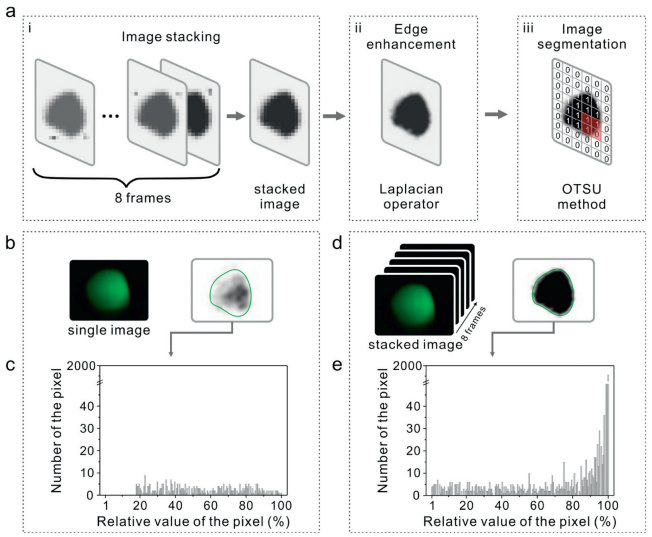

Fig. 2. (a) Schematic about how to digitize the FL exposures for multiplied sensitivity that divided into three major program procedures from left to right. The blankets of (b) and (d) are statistical analyses of only one layer and hyphenated multilayers, respectively. Below (c, e) are the corresponding histograms of pixel counts as a function of relative grey scale.

Moving forward, a single-channel spectrofluorimeter was configured to enact the previous piloted plan. Here as demonstrated in Fig. S5a (Supporting information), the design was debriefed as follows: An HONOR V20 mobile phone came at convenience by its 48-megapixel (8000 × 6000) rear camera for direct FL visualization. Next to it is a lightproof attachment of optical accessories, where the incident laser from the illuminator (488 nm, 20 mW) passes through the filter shedding excitation upon the sample cuvette. Of note, the power could be steadily retained ~100% over a benchmark test period as long as 300 min (0.789 mW/mm^2, 25 °C) as verified in Fig. S6 (Supporting information). Perpendicularly, the emergent ray gets collected *via* a piece of concave collimator, delivering the convergent spot on the lens (Fig. S5b in Supporting information). At the end of this pathway, the illumination was captured in a series of photos and saved in designated directory. To completely quarantine from the environmental stray lights, opaque plastics wrap all around the firmware cube.

By contrast to the conventional organization of hardware, the software "a functional App" was custom-developed in Java code. In relatively more details, it is capable of three primary modes: image acquisition, data archiving, and data processing (Fig. S7 in Supporting information). Stepwise speaking, the emission outputs were snapshotted upon touching the button of acquisition after adjusting to appropriate exposure (1/8) and ISO (6400) for consistently minimal back-ground. Pictures were saved instantaneously in a new folder, and subjected to quantitative treatment as diagrammatized in Fig. S8 (Supporting information).

As for the running principle, the App console would firstly direct the camera to shoot 8 consecutive frames in Video (Showlive) mode [34]. Subsequently, by overlapping each slide together as depicted in Fig. 2a (i), the greyscale of the signal regions went higher than that of the stochastically scattered noisy pixels, which suggests an intensified differentiation between the two averages of their summations over the photo pool, *i.e.*, an improved signal-to-noise ratio (SNR). Since true or false identification along the signal perimeter a poses critical issue to the overall measurement validity, the second stage mainly dealt with the so-called "object border check". Hereby, an edge-survey algorithm was employed with Laplacian operator as the kernel [35]. It screened the entire grid in an ergodic manner for fast intensity variation, resulting in a compensating "mask" of quality boundary information for the computed coordinate values in the previous step (Fig. 2a (ii)). Getting down to the third place, the imagery plane was compartmentalized into a binary matrix using the well-adopted Otsu's thresholding method [36] (Fig. 2a (iii)), where cells of target and background are assigned with 1 and 0, respectively. Any floating artefacts were removed.

To inspect the practical effectiveness of the above theory, a comparison in SNR was instantiated between one straightforward single FL shot (Fig. 2b left) and 8 frames (Fig. 2d left) in a group set after the introduction of 2 μmol/L CHL to the as-fabricated biosensor. As a follow-up, each visual transformation was paralleled aside on the right of Figs. 2b and d out of the foregoing progressive protocol. Clearly from the abundance distribution of normalized gray value of all pixels, one could easily catch that the brilliance by sum of plural photographs (Fig. 2c) indeed prevails over that of a mere singular one (Fig. 2e), tantamount to a 15-fold sensitization by global integral.

The phone-tandem mini-fluorophotometer was now ready for launch for the antibiotic quantitation. As delineated in Fig. 3a, in the absence of CHL the first target, the FL of fluorogenic P1 was statically extinguished due to SPR from the far-reaching protrusions of AuNB on the matched nearby. The thermos-dynamically favorable association with CHL would detach P1 from the overhang state to a folded motif that resumed the FL intensity [37]. Such photoluminescent kinetics was tracked up to a plateau within 25 min and by that, the optimum of AuNBs for bioconjugation was settled at 0.5 nmol/L (Fig. S9 in Supporting information). Abiding by this mechanism, the captured panel as expected in Fig. 3b manifested an escalating FL hotspot in the middle of the screen when the amount of CHL (C_{CHL}) rises from 0.05 μmol/L to 40 μmol/L. Fig. 3c plotted out the significant linearity between the calculated gradation and the titrant content with a calibration $I = 0.28 \cdot \lg C + 0.52$ and a regression coefficient $R^2 = 0.977$. The limit of detection (LOD) was also determined to be 9.6 nmol/L, lower than those recently devised approaches on the basis of fluorescence [3,14,15] and electrochemistry [3,16-18], while compara-

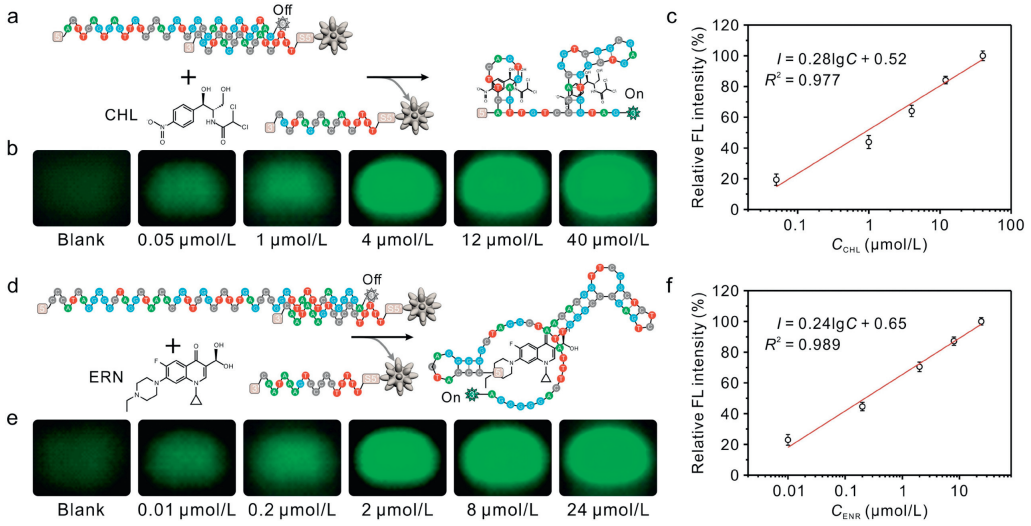

Fig. 3. Mobile mini-fluorometer for scanometric quantification of CHL (upper half) and ENR (lower half). (a, d) Conformational transition of tailored aptamer before and after its binding with the appointed analyte. (b, e) Digital sensor grams in correlation with varying target aliquots from low (left) to high (right) concentration in PBS. Calibration curve about the scaled C_{CHL} (c) and C_{ENR} (f) dependent FL irradiation. Error bars represent SD ($n = 3$).

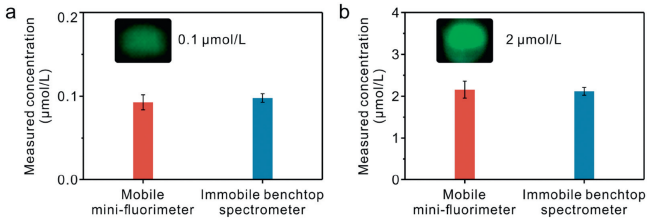

Fig. 4. Comparative fluorimetries on 0.1 μmol/L (a) and 2 μmol/L (b) CHL in spiked milk with both the mobile minifluorimeter (red) and the immobile benchtop spectrometer (blue).

ble to the colorimetric amplifications [22] (Table S2 in Supporting information). In order to evaluate the specificity of this aptaprobe, its responses to 10 μmol/L antibiotic interferents including erythromycin (ERY), florfenicol (FLO), gentamicin (GEN), thiamphenic (THI), kanamycin sulfate (KAN), streptomycin (STR), lincomycin hydrochloride (LIN) and neomycin (NEO) were examined concomitantly one by one in Fig. S10a (Supporting information), where the signal of CHL overwhelmed, underscoring the essential selectivity of the built-in methodology.

Moreover, as an applicative extension, another kind of overdosed antibiotics, enrofloxacin (ERN), was checked out. As showcased similarly in Fig. 3d, the annihilated FL from P3 was rekindled owing to its stronger tie with ERN [38]. Likewise in Figs. 3e and f, altogether they conveyed a sensitive and wide window toward C_{ERN} in the range of 0.01–24 μmol/L, plus an LOD down to 1.1 nmol/L that superior to the lately published optical [20,38-42], and electrochemical means [43–45] (Table S3 in Supporting information); one more word, its anti-interference potential seems also well enough among the family of homologues (Fig. S10b in Supporting information). Presumably from the two testees, the proposed ensemble could say a generic tool, which should be generalizable in the gamut of antibiotic probing regimes.

To confirm the reliability and accuracy of this gadget, recovery experiments were firstly carried out in the premixture of spiked milk with CHL, provided the fact that traces of CHL and ERN as certified veterinary drugs have early on presented in animal-derived milk, eggs and honey [46]. As displayed in red columns of Figs. 4a and b, the recoveries were 92.6% ± 5.4% for 0.1 μmol/L CHL and 106.1% ± 6.1% for 2 μmol/L. By reference to the traditional benchtop equipment (97.8% and 103.9% in blue, Figs. S11 and S12 in Supporting information), the correctiveness of our handheld readouts was testified commeasurable. Table S4 (Supporting information) compiled the appraisals for eggs and honey spikings that also exhibit satisfactory dataset: The recovery rates dwell within 94.7%–104.9% whereas RSD of 3.2%–5.7%, hence reflecting the mature status for real exercises.

In summary, a portable visualizer was crafted to handle the point-of-need antibiotic screening. Its machinery pivotal lies in the aptameric FL recovery after the AuNB-rallied photo-bleaching. Such simple strategic signaling was relayed *via* a streamlined framework of firmware. To secure a high-fidelity (hi-fi) but handy matter-to-math metrization, the open and cohesive intelligent handset was recruited to warp up both rapid acquisition and augmented recognition of CHL and ENR with remarkable equivalency to those professional intricate workstations in terms of precision and pragmaticality. The developed build is readily compatible with the whole series by alternating the archived interactome of antibiotic-bound P1 with their paired P2. Future coupling with disposable extractors, the diagnostic upgrade towards a multiplex (multifactor) analyzer would be definitely welcomed to dovetail the true market entry requirements at hand.

Declaration of competing interest

The authors declare that they have no known competing financial interests or personal relationships that could have appeared to influence the work reported in this paper.

Acknowledgments

This work was supported by National Natural Science Foundation of China (Nos. 21874071 and 22204077), China Postdoctoral Science Foundation (No. 2021M701722), and Fundamental Research Funds for the Central Universities (Nos. 30921013112 and 30922010501).

Supplementary materials

Supplementary material associated with this article can be found, in the online version, at doi:10.1016/j.cclet.2023.109036.

References

[1] N. Zhao, J.M. Liu, J.F.E. Yang, et al., ACS Appl. Bio Mater. 4 (2020) 995–1002.
[2] M. Tian, X.M. He, Y.Z. Feng, et al., Antibiotics 10 (2021) 539.
[3] X.Y. Yue, C.Y. Wu, Z.J. Zhou, L. Fu, Y.H. Bai, Foods 11 (2022) 3138.
[4] A. Bagheri Hashkavayi, J. Bakhsh Raoof, R. Ojani, E. Hamidi Asl, Electroanalysis 27 (2015) 1449–1456.
[5] T. Trouchon, S. Lefebvre, Open J. Vet. Med. 6 (2016) 40–58.
[6] D.Q. Li, M. Huang, Z.Y. Shi, et al., Anal. Chem. 94 (2022) 2996–3004.
[7] H.T. Lai, J.H. Hou, C.I. Su, C.L. Chen, Environ. Safe 72 (2009) 329–334.
[8] L. Serwecińska, Water 12 (2020) 3313.
[9] N.A. Khudzaifah, M.M.S. Basukiwardojo, World J. Adv. Res. Rev. 15 (2022) 525–533.
[10] O. Zelenina, V. Vlizlo, M. Kozak, et al., J. Appl. Pharm. Sci. 12 (2022) 068–075.
[11] W.M.A. Niessen, J. Chromatogr. A 812 (1998) 53–75.
[12] C.L. Flurer, Electrophoresis 18 (1997) 2427–2437.
[13] A. Luís, M. Héctor, S. Célia, et al., Crit. Rev. Food Sci. 56 (2016) 249–265.
[14] Z. Rahmati, M. Roushani, Microchim. Acta 189 (2022) 1–10.
[15] A. Amalraj, P. Perumal, Microchem. J. 173 (2022) 106971.
[16] Y.J. Li, H.P. Dai, N.N. Feng, et al., Mater. Express 9 (2019) 59–64.
[17] S. Pilehvar, D. Jambrec, M. Gebala, W. Schuhmann, K. De Wael, Electroanalysis 27 (2015) 1836–1841.
[18] R.R. Yang, J.L. Zhao, M.J. Chen, et al., Talanta 131 (2015) 619–623.
[19] X.J. Liu, H. Cheng, Y.C. Zhao, Y. Wang, F. Li, Biosens. Bioelectron. 199 (2022) 113906.
[20] P.P. Gai, C.C. Gu, T. Hou, F. Li, Anal. Chem. 89 (2017) 2163–2169.
[21] C.C. Chang, G. Wang, T. Takarada, M. Maeda, ACS Appl. Mater. Inter. 9 (2017) 34518–34525.
[22] C. Zhou, C.J. Sun, H.M. Zou, Y.X. Li, Food Chem. 377 (2022) 132031.
[23] S.J. Wu, Q.M. Chen, L.Q. Fu, et al., Anal. Sci. 38 (2022) 369–375.
[24] X.J. Liu, X. Gao, L.M. Yang, Y.C. Zhao, F. Li, Anal. Chem. 93 (2021) 11792–11799.
[25] H.J. Qi, L.X. Feng, S.X. Zhao, H.Y. Li, F. Li, Spectrochim. Acta A 284 (2023) 121758.
[26] I. Hernández-Neuta, F. Neumann, J. Brightmeyer, et al., J. Intern. Med. 285 (2019) 19–39.
[27] J.L. Shen, L. Liang, M.S. Xiao, et al., J. Am. Chem. Soc. 141 (2019) 11938–11946.
[28] X.W. Wang, L. Yan, Z.J. Yu, et al., ChemPlusChem 87 (2022) e202100479.
[29] A. Manjavacas, J.G. Liu, V. Kulkarni, P. Nordlander, ACS Nano 8 (2014) 7630–7638.
[30] P. Anger, P. Bharadwaj, L. Novotny, Phys. Rev. Lett. 96 (2006) 113002.
[31] C.M. Xue, O. Birel, M. Gao, et al., Phys. Chem. C 116 (2012) 10396.
[32] H.Z. Yu, M.S. Xiao, W. Lai, et al., Anal. Chem. 92 (2020) 4491–4497.
[33] X. Zhang, M.R. Servos, J.W. Liu, J. Am. Chem. Soc. 134 (2012) 7266–7269.
[34] J. Balsam, H.A. Bruck, Y. Kostov, A. Rasooly, Sens. Actuators B: Chem. 171 (2012) 141–147.
[35] P. Fan, R.G. Zhou, W.W. Hu, N.H. Jing, Quantum Inf. Process. 18 (2019) 1–23.
[36] F. Essaf, Y.J. Li, S. Sakho, P.K. Gadosey, T. Zhang, in: Proceedings of the 2020 6th International Conference on Computing and Artificial Intelligence, Tianjin, 2020, pp. 204–212.
[37] L.C. Wang, C.Y. Hong, Z.Z. Lin, X.M. Chen, Z.Y. Huang, Anal. Methods 12 (2020) 2391–2397.
[38] X. Shen, J.H. Chen, S.W. Lv, et al., Molecules 24 (2019) 4462.
[39] X.J. Guo, L.Z. Zhang, Z.W. Wang, et al., Spectrochim. Acta A 219 (2019) 15–22.
[40] J.X. Chen, F. Xu, H.Y. Jiang, et al., Food Chem. 113 (2009) 1197–1201.
[41] J.T. Dong, H.A. Li, P.C. Yan, et al., Microchim. Acta 186 (2019) 1–8.
[42] J.Y. Sha, H. Lin, V. Timira, J.X. Sui, Food Anal. Methods 14 (2021) 957–967.
[43] N. Karuppusamy, V. Mariyappan, S.M. Chen, R. Ramachandran, Nanoscale 14 (2022) 1250–1263.
[44] D. Jiang, M. Wei, X.J. Du, et al., Biosens. Bioelectron. 200 (2022) 113917.
[45] D.W. Wang, S.H. Jiang, Y.Y. Liang, et al., Talanta 236 (2022) 122835.
[46] T. Beyene, J. Vet. Sci. Technol. 7 (2016) 285.